

Fe(II) Mononuclear Complexes with a New Aminopyridyl Ligand Bearing a Pivaloylamido Arm. Preparation and Spectroscopic Characterizations of a Fe^{III}-Hydroperoxo Complex with Oxygen and Nitrogen Donors

Marlène Martinho,[†] Frédéric Banse,^{*†} Joëlle Sainton,[†] Christian Philouze,[‡] Régis Guillot,[†] Guillaume Blain,[†] Pierre Dorlet,[†] Sophie Lecomte,[§] and Jean-Jacques Girerd[†]

Institut de Chimie Moléculaire et des Matériaux d'Orsay, UMR 8182, Laboratoire de Chimie Inorganique, Université Paris-XI, 91405 Orsay Cedex, France, Laboratoire d'Etudes Dynamiques et Structurales de la Sélectivité, Service de Cristallographie, bât. Chimie Recherche, 301 Rue de la Chimie, DU BP 53, 38041 Grenoble Cedex 9, France, and LADIR, CNRS—Université Pierre et Marie Curie, UMR 7075, 2 rue Henri Dunant, F-94320 Thiais, France

Received December 7, 2006

Two new mononuclear Fe^{II} complexes, [(L₅²aH)Fe^{II}](PF₆)₂ (**1**-(PF₆)₂) and [(L₅²a)Fe^{II}]BPh₄ (**2**-(BPh₄)) have been synthesized with the new aminopyridyl ligand bearing a pivaloylamido arm L₅²aH (2,2-dimethyl-N-[6-([2-(methylpyridin-2-ylmethyl-amino)-ethyl]-pyridin-2-ylmethyl-amino)-methyl]-pyridin-2-yl]-propionamide), or its deprotonated form L₅²a⁻. The structures of the ferrous complexes have been determined by X-ray analysis. The mononuclear Fe^{II} is in a pseudo-octahedral environment in both complexes, the six positions around the metal center being occupied by five nitrogen atoms and one oxygen atom from the ligand. Whatever the protonation state of the amide function, the structures are very similar, the Fe^{II} being 6-fold coordinated by the two amines, three pyridines, and the oxygen atom from the ligand. These two complexes exhibit an acid/base equilibrium in solution that has been studied by UV–vis spectroscopy and cyclic voltammetry in acetonitrile. The reactivity of **1**-(PF₆)₂ with H₂O₂ in methanol affords the formation of a new low-spin Fe^{III}(OOH) intermediate in which the oxygen atom is retained in the coordination sphere of the metal.

Introduction

Dioxygen is activated by non-heme biological systems to carry out selective transformations of organic substrates.^{1–3} Key intermediates, such as Fe^{III}(η¹-hydroperoxo), Fe^{III}(η²-peroxo), and Fe^{IV}(oxo), have been identified in bleomycin,⁴ naphthalene dioxygenase,⁵ or taurine/α-ketoglutarate dioxygenase.⁶ Considerable efforts have been devoted to prepare and characterize models of these transients. Amine/pyridine

ligands have been frequently used and have allowed the identification of synthetic models of the above intermediates.^{2,7} More elaborate ligands containing amidate functions^{8,9} or rigid backbones such as bispidine¹⁰ have also been used to prepare Fe^{III}(OOH) complexes.

In order to model the supramolecular effects provided by the hydrogen-bond network in many proteins, Borovik and co-workers have developed a series of tripodal urea-based ligands that have allowed the formation of Fe^{III} complexes with terminal oxo ligands.¹¹ Wada et al. used an amine/

* To whom correspondence should be addressed. E-mail: fredbanse@icmo.u-psud.fr.

[†] Université Paris-XI.

[‡] Service de Cristallographie, bât.

[§] CNRS—Université Pierre et Marie Curie.

(1) Baik, M. H.; Newcomb, M.; Friesner, R. A.; Lippard, S. J. *Chem. Rev.* **2003**, *103*, 2385–2419.

(2) Costas, M.; Mehn, M. P.; Jensen, M. P.; Que, L. *Chem. Rev.* **2004**, *104*, 939–986.

(3) Zhang, J.; Zheng, H.; Groce, S. L.; Lipscomb, J. D. *J. Mol. Catal. A* **2006**, *251*, 54–65.

(4) Burger, R. M. *Struct. Bond.* **2000**, *97*, 287–303.

(5) Karlsson, A.; Parales, J. V.; Parales, R. E.; Gibson, D. T.; Eklund, H.; Ramaswamy, S. *Science* **2003**, *299*, 1039–1042.

(6) Riggs-Gelasco, P. J.; Price, J. C.; Guyer, R. B.; Brehm, J. H.; Barr, E. W.; Bollinger, J. M.; Krebs, C. J. *Am. Chem. Soc.* **2004**, *126*, 8108–8109.

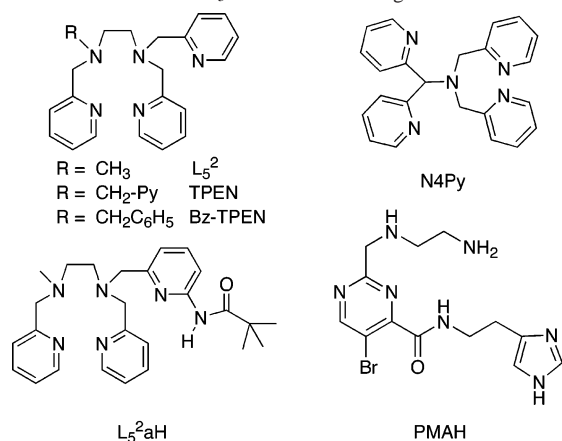
(7) Girerd, J. J.; Banse, F.; Simaan, A. J. *Struct. Bond.* **2000**, *97*, 145–177.

(8) Guajardo, R. J.; Hudson, S. E.; Hudson, S. J.; Mascharak, P. J. *J. Am. Chem. Soc.* **1993**, *115*, 7971–7977.

(9) Lippai, I.; Magliozzo, R. S.; Peisach, J. J. *Am. Chem. Soc.* **1999**, *121*, 780–784.

(10) Bukowski, M. R.; Comba, P.; Limberg, C.; Merz, M.; Que, L.; Wistuba, T. *Angew. Chem., Int. Ed.* **2004**, *43*, 1283–1287.

(11) Borovik, A. S. *Acc. Chem. Res.* **2005**, *38*, 54–61.

Scheme 1. Structure of L_5^2 aH and Related Ligands

pyridine tripodal ligand with pivaloylamido groups to prepare an $Fe^{III}(\text{OOH})$ complex that exhibited a high-spin state ($S = 5/2$) unlike the other models.¹² In their case, it is likely that the polar groups did not form hydrogen bonds in the metal environment but provided sterical hindrance instead.

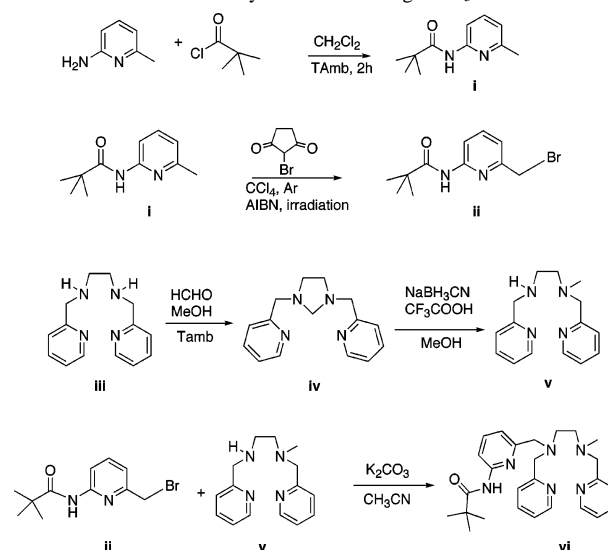
Que et al. have also reported ligands with amide groups for a different purpose. They prepared complexes in which the amide carbonyl oxygen was tightly bound to iron, in order to mimic more closely the mixed N–O metal environment encountered in numerous non-heme iron enzymes.^{13,14}

In this paper, we report the results obtained with the ligand L_5^2 aH (2,2-dimethyl-*N*-[6-([2-(methyl-pyridin-2-ylmethyl-amino)-ethyl]-pyridin-2-ylmethyl-amino)-methyl]-pyridin-2-yl]-propionamide) (cf. Scheme 1). This new ligand was obtained by a moderate modification of L_5^2 , our prototypical ligand for the preparation of $S = 1/2$ $Fe^{III}(\text{OOH})$. It allows the formation of two Fe^{II} complexes that exhibit an acid/base equilibrium in solution. One of these Fe^{II} species is the precursor of a $S = 1/2$ $Fe^{III}(\text{OOH})$ intermediate in which the metal center is in an uncommon 4-N-1-O ancillary environment.

Results and Discussion

Synthesis of the Ligand. The ligand L_5^2 aH (cf. Scheme 1) was obtained by following a multistep synthesis as described in Scheme 2.

Compounds **i** and **ii** were obtained by following the procedure described by Harata et al.¹⁵ Compound **i** was obtained quantitatively by alkylation of 2-amino-6-methylpyridine with pivaloyl chloride in the presence of triethylamine. Bromation of **i** was carried out by adding *N*-bromosuccinimide and AIBN in boiling tetrachloromethane under argon and irradiation to afford **ii**. Imidazolidine derivative **iv** was obtained from *N,N'*-bis(2-pyridylmethyl)-1,2-diaminoethane (**iii**) and HCHO in methanol. Compound **v** was prepared from compound **iv** quantitatively by reduction in

Scheme 2. Schematized Synthesis of the Ligand L_5^2 aH

presence of $NaBH_3CN$ and CF_3COOH following the method of Baffert et al.¹⁶ Then, the reaction of **v** and **ii** in the presence of K_2CO_3 in acetonitrile provided the ligand L_5^2 aH (**vi**).

The full details and characterizations for each product are given in the Experimental Section.

Structures of $[(L_5^2aH)Fe^{II}](PF_6)_2$ (1**- $(PF_6)_2$) and $[(L_5^2a)Fe^{II}]BPh_4$ (**2**- (BPh_4)).** The reaction of an Fe^{II} salt with L_5^2 aH in neutral or alkaline conditions allowed the isolation of two different complexes that have been recrystallized (cf. Experimental Section). The structures of the complex cations $[(L_5^2aH)Fe^{II}]^{2+}$ and $[(L_5^2a)Fe^{II}]^+$ are shown in Figures 1 and 2, respectively. A selection of bond distances and angles is reported in Table 1.

The mononuclear Fe^{II} is in a pseudo-octahedral environment in both complexes, the six positions around the metal center being occupied by five nitrogen atoms and one oxygen atom from the ligand. The equatorial positions are occupied by the two amino functions, one pyridine and the pivaloyl oxygen atom, whereas the apical positions are occupied by two pyridines, one bearing the pivaloyl function. The two structures are therefore similar at first sight.

The $Fe-N$ distances (2.136(3)–2.211(4) Å for **1**- $(PF_6)_2$ and 2.128(2)–2.238(2) Å for **2**- (BPh_4)) are typical of high-spin Fe^{II} metal centers. They are similar to those observed by Mialane et al.¹⁷ and Bernal et al.¹⁸ for the complexes $[(L_5^2)Fe(H_2O)](BPh_4)_2$ and $[(L^1)Fe(H_2O)](PF_6)_2$ ¹⁹, respectively (L^1 and L_5^2 are amine/pyridine-containing ligands, the structure of L_5^2 is shown in Scheme 1). Whatever the protonation state of the ligand, the amide function is coordinated to the Fe^{II} by its oxygen atom. This forms a six-membered metalocycle with the adjacent pyridine. In

- (12) Wada, H.; Ogo, S.; Nagatomo, S.; Kitagawa, T.; Watanabe, Y.; Jitsukawa, K.; Masuda, H. *Inorg. Chem.* **2002**, *41*, 616–618.
 (13) Mandal, S. K.; Que, L. *Inorg. Chem.* **1997**, *36*, 5424–5425.
 (14) Oldenburg, P. D.; Shteinman, A. A.; Que, L. *J. Am. Chem. Soc.* **2005**, *127*, 15672–15673.
 (15) Harata, M.; Jitsukawa, K. M. H.; Einaga, H. *Chem. Lett.* **1995**, 61–62.

- (16) Baffert, C.; Collomb, M. N.; Deronzier, A.; Kjaergaard Knudsen, S.; Latour, J. M.; Lund, K. H.; McKenzie, C. J.; Mortensen, M.; Nielsen, L.; Thorup, N. *Dalton Trans.* **2003**, 9, 1765–1772.
 (17) Mialane, P.; Novorokjine, A.; Pratiel, G.; Azéma, L.; Slany, M.; Godde, F.; Simaan, A.; Banse, F.; Kargar-Grisel, T.; Bouchoux, G.; Sainton, J.; Horner, O.; Guilhem, J.; Tchertanova, L.; Meunier, B.; Girerd, J. J. *Inorg. Chem.* **1999**, *38*, 1085–1092.
 (18) Bernal, I.; Jensen, I. M.; Jensen, K. B.; McKenzie, C. J.; Toftlund, H.; Tuchagues, J. P. *J. Chem. Soc., Dalton Trans.* **1995**, 3667–3675.

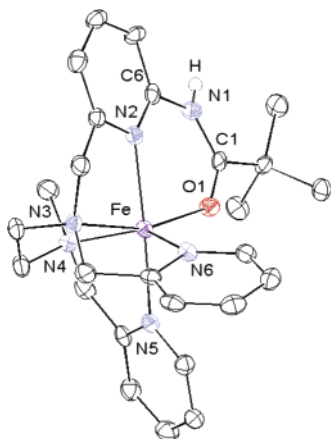


Figure 1. ORTEP drawing of $[(L_5^2aH)Fe^{II}]^{2+}$. Ellipsoids are drawn at the 50% probability level.

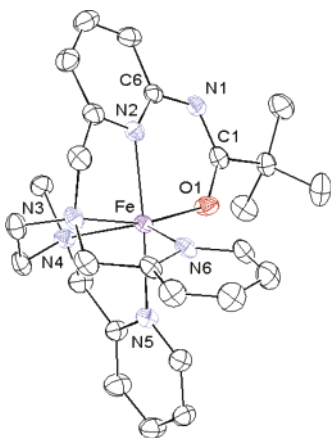


Figure 2. ORTEP drawing of $[(L_5^2a)Fe^{II}]^+$. Ellipsoids are drawn at the 50% probability level.

both complexes, the shortest bond is the iron–oxygen one. This has been observed recently by Oldenburg et al.¹⁴ (2.0431(17) Å) for an Fe^{II} complex with a benzamide containing ligand and by Wada et al.²⁰ for the complex $[Fe^{III}(bppa)(tBuCOO)]^{2+}$ (2.095(7) and 2.071(6) Å).¹⁹ The iron–oxygen bond distance is particularly short in complex **2** (1.959(2) Å for **2-BPh₄** and 2.009(3) Å for **1-(PF₆)₂**). A perusal of the values listed in Table 1 shows some differences regarding the pivaloylamido moiety in each complex. The protonation of the pivaloylamido function in complex **1** implies a longer N₁–C₁ bond (1.327(6) Å) than in complex **2** (1.303(3) Å). In parallel, the O₁–C₁ bond is shorter in complex **1** (1.244(5) Å) than in complex **2** (1.290(3) Å).

(19) Abbreviations used. BLM, bleomycin; TPEN, *N,N,N',N'*-tetrakis(2-pyridylmethyl)-1,2-diaminoethane; L₅², *N*-methyl-*N,N,N'*-tris(2-pyridylmethyl)-1,2-diaminoethane; L₅³, *N*-methyl-*N,N,N'*-tris(2-pyridylmethyl)-1,2-diaminopropane; Bz-TPEN, *N*-benzyl-*N,N,N'*-tris(2-pyridylmethyl)-1,2-diaminoethane; L¹, *N,N'*-bis(6-methyl-2-pyridylmethyl)-*N,N'*-bis(2-pyridylmethyl)-1,2-diaminoethane; bppa, bis(6-pivalamido-2-pyridylmethyl)(2-pyridylmethyl)amine; N4Py, *N,N*-bis(2-pyridylmethyl)-bis(2-pyridyl)methylamine; PMAH, 2-(2',5'-diazapentyl)-5-bromopyrimidine-6-carboxylic acid *N*-[2-(4'-imidazolyl)ethyl]amide; Py5, 2,6-bis(methoxy(di(2-pyridyl)methyl)pyridine); L₂, 1,5-bis(methoxycarbonyl)-3-methyl-2,4-bis(2-pyridyl)-7-(2-pyridylmethyl)-3,7-diazabicyclo(3.3.1)nonan-9-one; L₃, 1,5-bis(methoxycarbonyl)-7-methyl-2,4-bis(2-pyridyl)-3-(2-pyridylmethyl)-3,7-diazabicyclo(3.3.1)nonan-9-one.

(20) Wada, H.; Ogo, S.; Watanabe, Y.; Mukai, M.; Kitagawa, T.; Jitsukawa, K.; Masuda, H.; Einaga, H. *Inorg. Chem.* **1999**, *38*, 3592–3593.

Table 1. Selected Bond Distances (Å) and Angles (deg) for the Complexes $[(L_5^2aH)Fe^{II}](PF_6)_2$ (**1-(PF₆)₂**) and $[(L_5^2a)Fe^{II}]BPh_4$

	$[(L_5^2aH)Fe^{II}](PF_6)_2$	$[(L_5^2a)Fe^{II}]BPh_4$
Fe ₁ –O ₁	2.009(3)	1.959(2)
Fe ₁ –N ₂	2.147(4)	2.128(2)
Fe ₁ –N ₃	2.195(3)	2.234(2)
Fe ₁ –N ₄	2.211(4)	2.238(2)
Fe ₁ –N ₅	2.207(4)	2.226(2)
Fe ₁ –N ₆	2.136(3)	2.158(2)
O ₁ –C ₁	1.244(5)	1.290(3)
N ₁ –C ₁	1.327(6)	1.303(3)
O ₁ –Fe ₁ –N ₂	83.70(12)	84.92(8)
O ₁ –Fe ₁ –N ₄	102.52(12)	106.27(8)
O ₁ –Fe ₁ –N ₅	92.01(12)	90.64(8)
O ₁ –Fe ₁ –N ₆	105.86(13)	105.27(8)
N ₃ –Fe ₁ –N ₄	81.66(13)	79.02(8)

From these observations we can conclude that, in **2**, the N₁–C₁ has a double bond character and the negative charge is delocalized on O₁. Such a modification upon deprotonation of a pivaloylamido substituent has been recently proposed for a Zn(II) complex.²¹

UV–Visible Spectroscopy. The molecular complexes **1** and **2** have been studied by UV–vis absorption spectroscopy.

The UV–vis spectra of **1-(BPh₄)₂** were recorded in acetonitrile and methanol, and are similar in both solvents. They exhibit a band at $\lambda_{max} = 393$ nm ($\epsilon = 1800$ M^{–1} cm^{–1} in acetonitrile and $\epsilon = 1630$ M^{–1} cm^{–1} in methanol) with a shoulder at ca. 455 nm. This broad absorption can be assigned to metal-to-ligand charge transfers (MLCT) as mentioned previously for Fe^{II} complexes bearing amine/pyridine ligands.^{17,18} The extinction coefficient is typical of a high-spin Fe^{II} complex. Since the spectra are similar in both solvents, it is quite clear that the structure determined in the solid state is preserved in solution, i.e., with L₅²aH acting as an hexadentate ligand.

The UV–vis spectrum of **2-BPh₄** in acetonitrile exhibits a similar band at $\lambda_{max} = 431$ nm ($\epsilon = 1850$ M^{–1} cm^{–1}). As for complex **1**, this band can be assigned to a MLCT for a high-spin Fe^{II} complex. From **1** to **2**, the oxygen atom of the amido function turns from σ donor to σ and π donor. As a consequence, the MLCT band decreases in energy when one goes from **1** to **2**.

Equilibrium between 1 and 2. Since the protonation state of the ligand allows the formation of two distinct Fe^{II} complexes, the conversion between both complexes was studied by UV–vis spectroscopy upon acid or base treatment.

By adding diisopropylethylamine progressively (up to 1 equiv vs Fe) to an acetonitrile solution of **1-(BPh₄)₂** at room temperature, the intensity of the MLCT band of **1** decreases whereas that of **2** increases (cf. Figure 3). The presence of isosbestic points at 360 and 418 nm reveals that there is a direct conversion from **1** to **2**. By considering the absorbance variation at 393 nm, the pK_a of the acid/base equilibrium between **1** and **2** can be estimated to be ca. 20.5 at room temperature. The reaction is not quantitative in these conditions since diisopropylethylamine is a weaker base (pK_a = 18.1 in acetonitrile²²) than **2**.

(21) Szajna, E.; Makowska-Grzyska, M. M.; Wasden, C. C.; Arif, A. M.; Berreau, L. M. *Inorg. Chem.* **2005**, *44*, 7595–605.

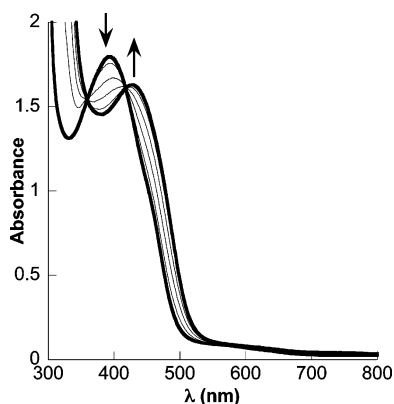


Figure 3. Conversion of **1** (1 mM in acetonitrile, room temperature) to **2** monitored by UV-vis, upon addition of 0.2, 0.4, 0.6, 0.8, and 1 equiv of diisopropylethylamine.

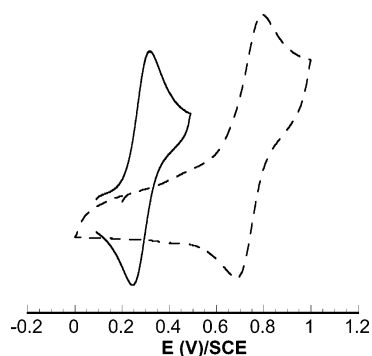


Figure 4. Cyclic voltammograms in acetonitrile at $-20\text{ }^{\circ}\text{C}$ of an equimolar mixture of $\text{L}_5^2\text{aH} + \text{Fe}^{\text{II}}(\text{OTf})_2 \cdot 2\text{CH}_3\text{CN}$ (**1**) (---) (scan rate 200 mV s^{-1}); and of $[\text{L}_5^2\text{aFe}^{\text{II}}]\text{BPh}_4$ (**2-BPh}_4**) (—) (scan rate 100 mV s^{-1}).

When HClO_4 was added to a solution of **2-BPh}_4, complex **1** could be obtained. However, clean isosbestic points were not observed in this case. The transformation was not neat in these conditions (see Cyclic Voltammetry section below).**

When 1–3 equiv of perchloric acid were added to an acetonitrile solution of **1-(BPh}_4)_2**, the shape of the absorption band at 393 nm, as well as its shoulder at 455 nm, were not modified. However, in such acidic conditions the protonation and further decoordination of the ligand led to the decrease of these features. The shoulder at 455 nm observed in the UV-vis spectrum of **1-(BPh}_4)_2** is then due to an intrinsic charge transfer of this complex. There is no spontaneous equilibrium between **1** and **2** in acetonitrile.

Cyclic Voltammetry. The electrochemical properties of the complexes **1** and **2** were investigated by cyclic voltammetry at $-20\text{ }^{\circ}\text{C}$ in acetonitrile.

The cyclic voltammogram (CV) of an equimolar mixture of L_5^2aH and $\text{Fe}^{\text{II}}(\text{OTf})_2 \cdot 2\text{CH}_3\text{CN}$ in acetonitrile displays a quasi-reversible wave at $E_{1/2} = 0.74\text{ V/SCE}$ (cf. Figure 4). This quasi-reversible wave corresponds to the $\text{Fe}^{\text{III}}/\text{Fe}^{\text{II}}$ couple. This large value is consistent with the stability of complex **1** toward air oxidation.

The CV of **1-(BPh}_4)_2** exhibits the same electrochemical feature, except for the presence of an intense irreversible

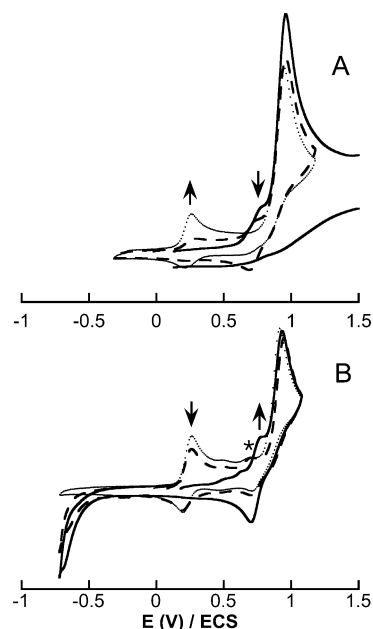


Figure 5. (A) Addition of (---) 0.2, and (\cdots) 0.6 equiv of TBA(OH) to **1-(BPh}_4)_2** (—) monitored by cyclic voltammetry at $-20\text{ }^{\circ}\text{C}$, Scan rate: 100 mV s^{-1} . (B) Addition of (---) 1 and (—) 2 equiv of HClO_4 to **2-BPh}_4** (\cdots); $T = -20\text{ }^{\circ}\text{C}$, Scan rate: 100 mV s^{-1} . The asterisk indicates the weak anodic process at 0.69 V, as indicated in the text.

anodic process at ca. 0.9 V/SCE which corresponds to the oxidation of the BPh_4^- anions.²³

The $\text{Fe}^{\text{III}}/\text{Fe}^{\text{II}}$ redox process of complex **2-BPh}_4** is quasi-reversible, the wave being at a lower potential ($E_{1/2} = 0.28\text{ V/SCE}$) (cf. Figure 4). The relative values of the potentials observed for **1** and **2** are consistent with the overall charge of the complexes, that is, dicationic for **1** and monocationic for **2**.

Equilibrium between 1 and 2. The acid–base equilibrium between the two complexes was also studied by electrochemistry.

Upon addition of TBA(OH) (1 mM in methanol) to a solution of **1-(BPh}_4)_2** in acetonitrile at low temperature, the $\text{Fe}^{\text{II}} \rightarrow \text{Fe}^{\text{III}}$ wave at 0.74 V/SCE decreases in intensity. At the same time, the intensity of the wave at 0.28 V/SCE increases (cf. Figure 5A).

As shown in Figure 5B, the reverse phenomenon is observed. When **2** is treated by HClO_4 , **1** is formed. However, it seems that this reaction is complicated by other reactions, i.e., rearrangement of the coordination sphere of Fe, since a weak anodic wave at 0.69 V/SCE is observed during the conversion from **2** to **1**.

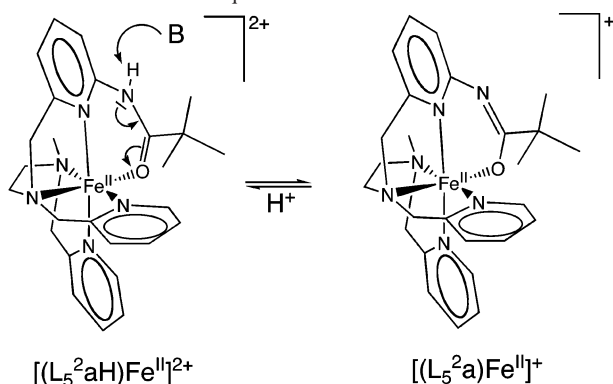
Basically, these changes confirm the conclusions drawn from UV-vis: **1** and **2** are predominant in solution in acidic or alkaline conditions, respectively.

The acid/base equilibrium between complexes **1** and **2** deduced from the experimental observations described above is depicted in Scheme 3. It is thus proposed that the acid/base reaction is accompanied by a displacement of electron pairs in the pivaloylamino substituent.

(22) Kelly-Rowley, A. M.; Lynch, M. V.; Anslyn, E. V. *J. Am. Chem. Soc.* **1995**, *117*, 3438–3447.

(23) Bancroft, E. E.; Blount, H. N.; Janzen, E. G. *J. Am. Chem. Soc.* **1979**, *101*, 3692–3694.

Scheme 3. Acid/Base Equilibrium between 1 and 2



Reaction of 1 with H₂O₂. (i) Identification of a Low-Spin Fe^{III}–OOH Intermediate. The reaction of 1 with an excess of hydrogen peroxide gave rise to a transient purple-reddish color. This sample was studied by UV–vis absorption spectroscopy and X-band EPR spectroscopy. By contrast, no transient was observed starting from complex 2.

Addition of a 100-fold excess of H₂O₂ (35% in water) to 1-(PF₆)₂ or to an equimolar solution of L₅²aH and Fe^{II}(OTf)₂·6H₂O (C_{Fe} = 1 mM) was carried out in methanol at –20 °C. The reaction monitored in time by UV–vis is shown in Figure 6. At the beginning, the MLCT absorption band of the Fe^{II} precursor decreases in intensity with the concomitant increase of two weak bands at 515 and 700 nm. The band at 700 nm reaches its maximum in 8 min. This latter chromophore is then converted to the 515 nm one as revealed by the isosbestic point at 610 nm. The band at λ_{max} = 515 nm reaches its maximum after ~1 h.

The absorption at 515 nm is characteristic of a low-spin Fe^{III}(OOH) complex. By comparison with several non-heme low-spin Fe^{III}–OOH complexes (cf. Table 2)^{7,24–26} the band at 515 nm can be attributed to a hydroperoxo-to-Fe^{III} charge transfer for the complex formulated as [(L₅²aH)Fe^{III}(OOH)]²⁺.

An aliquot of the above sample was taken at the maximum intensity of the 515-nm chromophore and studied by X-band EPR. The *g* = 2 region of the spectrum, where low-spin Fe^{III} complexes resonate, is shown in Figure 7.

This spectrum exhibits a rhombic signal with the following *g* values: *g*₁ = 2.23; *g*₂ = 2.16; *g*₃ = 1.96. These values are similar to those reported for all the non-heme low-spin Fe^{III}(OOH) species.^{2,7,27} This supports the attribution of the absorption band at 515 nm to [(L₅²aH)Fe^{III}(OOH)]²⁺. Quantification of this EPR spectrum by double integration leads to a yield of 48% in FeOOH. The extinction coefficient that

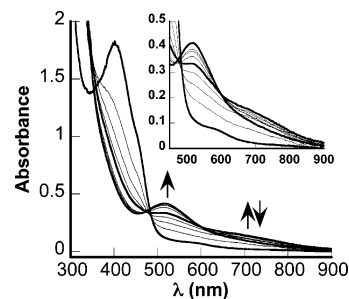


Figure 6. Reaction of an equimolar mixture of L₅²aH + Fe^{II}(OTf)₂·6H₂O (C_{Fe} = 1 mM in methanol) with H₂O₂ (100 equiv vs Fe) followed by UV–vis at –20 °C. The inset focuses on the conversion between the 700- and 515-nm chromophores.

is deduced for the 515-nm band (1100 M^{–1} cm^{–1}) is then very close to those reported for low-spin non-heme FeOOH complexes.

A signal at *g* = 4.3 is also present in our samples. This resonance at *g* = 4.3 is characteristic of rhombic high-spin Fe^{III} complexes and is generally attributed to degradation products.²⁸ Spectroscopic data reported for other low-spin FeOOH complexes are given in Table 2 for comparison.

In order to definitely confirm the assignment of the 515 nm absorption band to [(L₅²aH)Fe^{III}(OOH)]²⁺ resonance Raman spectroscopy was performed with an excitation at 568.2 nm. The spectrum displays bands in the 550–630 and 750–850 cm^{–1} regions, which are expected to include the iron–oxygen and oxygen–oxygen stretching modes (Figure 8). The former region displays a sharp band at 622 cm^{–1}. The second part of the spectrum displays a band at 795 cm^{–1}. Upon warming, the bands at 622 and 795 cm^{–1} decrease in intensity, reflecting the transient nature of the species. The band at 622 cm^{–1} is similar to that attributed to the Fe–O stretching mode for Fe^{III}(OOH) complexes obtained with amine/pyridine ligands (Table 2). The band at 795 cm^{–1} is similar to that reported for the O–O stretching modes in related complexes. The bands at 622 and 795 cm^{–1} are therefore attributed to the Fe–O and O–O stretching modes of [(L₅²aH)Fe^{III}(OOH)]²⁺, respectively.

(ii) Proposed Structure for [(L₅²aH)Fe^{III}(OOH)]²⁺. It has already been observed that the higher the number of pyridines bound to the Fe^{III}, the lower in energy the charge transfer.⁷ This is emphasized by the values in Table 2. Assuming that the metal center is 6-fold coordinated, there are, five, four, and three Fe–pyridine bonds in the FeOOH complexes with the ligands Py5, N4Py, and L₅² or TPEN,

- (24) Roelfes, G.; Lubben, M.; Chen, K.; Ho, R. Y. N.; Meetsma, A.; Genseberger, S.; Hermant, R. M.; Hage, R.; Mandal, S. K.; Young, V. G.; Zang, Y.; Kooijman, H.; Spek, A. L.; Que, L.; Feringa, B. L. *Inorg. Chem.* **1999**, *38*, 1929–1936.
- (25) Balland, V.; Banse, F.; Anxolabehere-Mallart, E.; Ghiladi, M.; Mattioli, T. A.; Philouze, C.; Blondin, G.; Girerd, J. J. *Inorg. Chem.* **2003**, *42*, 2470–2477.
- (26) Balland, V.; Banse, F.; Anxolabehere Mallart, E.; Nierlich, M.; Girerd, J. J. *Eur. J. Inorg. Chem.* **2003**, *13*, 2529–2535.
- (27) Solomon, E. I.; Brunold, T. C.; Davis, M. I.; Kemsley, J. N.; Lee, S.-K.; Lehnert, N.; Neese, F.; Skulan, A. J.; Yang, Y.-S.; Zhou, J. *Chem. Rev.* **2000**, *100*, 235–349.

- (28) Simaan, A. J.; Banse, F.; Girerd, J. J.; Wieghardt, K.; Bill, E. *Inorg. Chem.* **2001**, *40*, 6538–6540.
- (29) Burger, R. M.; Horwitz, C. P.; Peisach, J.; Wittenberg, J. B. *J. Biol. Chem.* **1979**, *254*, 12299–12302.
- (30) Simaan, A. J. Ph.D. thesis, Paris XI, 2000.
- (31) Simaan, A. J.; Dopner, S.; Banse, F.; Bourcier, S.; Bouchoux, G.; Boussac, A.; Hildebrandt, P.; Girerd, J. J. *Eur. J. Inorg. Chem.* **2000**, *7*, 1627–1633.
- (32) Lubben, M.; Meetsma, A.; Wilkinson, E. C.; Feringa, B.; Que, L. *Angew. Chem., Int. Ed. Engl.* **1995**, *34*, 1512–1514.
- (33) Roelfes, G.; Vrajmasu, V.; Chen, K.; Ho, R. Y. N.; Rohde, J. U.; Zondervan, C.; la Crois, R. M.; Schudde, E. P.; Lutz, M.; Spek, A. L.; Hage, R.; Feringa, B. L.; Munck, E.; Que, L. *Inorg. Chem.* **2003**, *42*, 2639–2653.
- (34) deVries, M. E.; LaCrois, R. M.; Roelfes, G.; Kooijman, H.; Spek, A. L.; Hage, R.; Feringa, B. L. *Chem. Commun.* **1997**, 1549–1550.

Table 2. Spectroscopic Characteristics of Some Low-Spin Fe^{III}(OOH) Complexes

	λ_{\max} (nm)	ϵ (M ⁻¹ cm ⁻¹)	<i>g</i> values	ν_{OO} (cm ⁻¹)	ν_{FeO} (cm ⁻¹)	refs
(BLM)Fe ^{III} (OOH)	—	—	2.26; 2.17; 1.94	—	—	29
[(L ₅ ² aH)Fe ^{III} (OOH)] ²⁺	515	1100 ^a	2.23; 2.16; 1.96	795	622	this work
[(L ₅ ²)Fe ^{III} (OOH)] ²⁺	537	1000	2.19; 2.12; 1.95	796	617	17,18
[(TPEN)Fe ^{III} (OOH)] ²⁺	541	900	2.22; 2.15; 1.997	796	617	30,31
[(N4Py)Fe ^{III} (OOH)] ²⁺	548	1200	2.17; 2.12; 1.98	790	632	24,32,33
[(Py5)Fe ^{III} (OOH)] ²⁺	592	—	2.15; 2.13; 1.98	806	627	33,34

^a Value deduced by double integration of the EPR spectrum.

Table 3. Crystallographic Data for Complexes **1** and **2**

	[(L ₅ ² aH)Fe ^{II}](PF ₆) ₂ (1)	[(L ₅ ² a)Fe ^{II}]BPh ₄ (2)
formula	[C ₂₆ H ₃₄ FeN ₆ O]P ₂ F ₁₂	[C ₂₆ H ₃₃ FeN ₆ O]C ₂₄ H ₂₀ B
fw	792.38	820.67
cryst syst	orthorhombic	triclinic
space group	<i>Pbca</i>	<i>P</i> $\bar{1}$
<i>a</i> [Å]	15.7239(6)	12.014(4)
<i>b</i> [Å]	17.8337(6)	13.001(3)
<i>c</i> [Å]	22.6661(9)	14.843(9)
α [°]	90	88.72(2)
β [°]	90	80.21(3)
γ [°]	90	69.60(2)
<i>V</i> [Å ³]	6355.9(4)	2140(2)
<i>Z</i>	8	2
<i>F</i> (000)	3232	868
λ [Å]	0.71073	0.71073
<i>T</i> [K]	100(1)	150(1)
ρ_{calcd} [Mg m ⁻³]	1.656	1.274
μ (Mo K α) [mm ⁻¹]	0.679	0.397
cryst size [mm ³]	0.12 \times 0.09 \times 0.06	0.34 \times 0.23 \times 0.17
θ range [deg]	1.80–24.72	3.03–30.00
no. of data collected	30 044	45 827
no. of unique data	5417	12 403
<i>R</i> (int)	0.08	0.13
abs correction	Sadabs	None
no. of params	441	532
no. of obsd reflns ^a	3434	7733
<i>R</i> ^b obsd	0.0505	0.0652
<i>R</i> _w ^c obsd	0.1057	0.0921
<i>S</i>	1.003	0.955
(Δ/ρ) _{max, min} [e Å ⁻³]	0.7, –0.53	0.80, –1.01

^a Data with $F_o > 4\sigma(F_o)$. ^b $R = \sum ||F_o| - |F_c|| / \sum |F_o|$. ^c $R_w = [\sum w(|F_o| - |F_c|)^2]^{1/2} / \sum w|F_o|^2$.

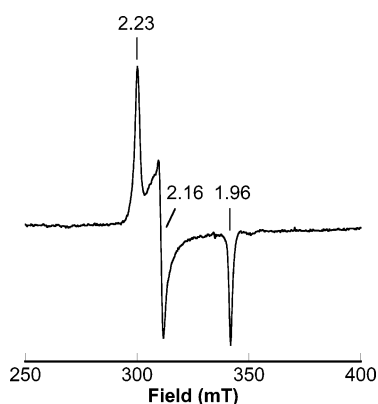


Figure 7. X-EPR spectrum of an equimolar mixture of L₅²aH + Fe^{II}(OTf)₂·6H₂O (*C*_{Fe} = 1 mM in methanol) with H₂O₂ (100 equiv vs Fe) recorded at 100 K. Experimental conditions: microwave frequency, 9.384 GHz; power, 2 mW; modulation, 0.5 mT/100 kHz.

respectively. Along this line, we propose that the [(L₅²aH)-Fe^{III}(OOH)]²⁺ complex may have a structure with only two pyridines coordinated to the metal center. The coordination sphere would then contain the two amino groups of the ethylenediamine moiety, one pyridyl arm, and the pyridine

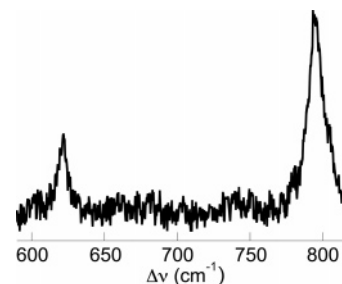


Figure 8. Resonance Raman spectrum of L₅²aH + Fe^{II}(OTf)₂·6H₂O (*C*_{Fe} = 1 mM in methanol) + 100 equiv of H₂O₂ recorded at –80 °C with excitation at 568.2 nm.

and oxygen atom of the pivaloylamido-pyridyl fragment. This latter fragment is likely to remain coordinated since it forms two adjacent chelate rings.

In the past,⁷ we have analyzed the *g* values of low-spin non-heme FeOOH complexes in the framework of the Griffith–Taylor model.^{35,36} In such *S* = 1/2 complexes, spin–orbit coupling and distortion from octahedral geometry partially lift the degeneracy of the ²T_{2g} state and three Kramers doublets are obtained. At 100 K, only the ground Kramers doublet is populated. For the 3d orbitals that contains the five electrons, the corresponding energetic situation is shown in Scheme 4. Convenient expressions of the two wave functions of the ground doublet and of the associated *g* values have been given by Taylor (see Supporting Information). These expressions have allowed us to compute *V*/ λ and Δ/λ , where *V* and Δ represent the rhombic and axial distortion energy, respectively, and λ the spin–orbit coupling constant. The coefficients *a*, *b*, and *c* of the wavefunctions of the resonating Kramers doublet have also been obtained and have revealed that the unpaired electron is in an orbital with a strong d_{xy} character.

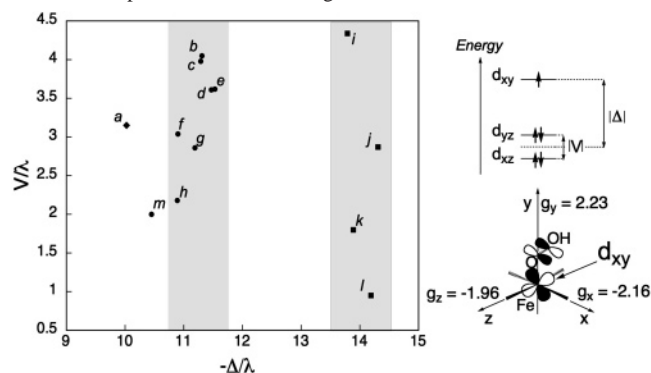
The same approach can be implemented here for [(L₅²aH)-Fe^{III}(OOH)]²⁺. In Scheme 4 is represented *V* as a function of $-\Delta$, for several *S* = 1/2 FeOOH complexes with amine/pyridine neutral ligands. It is clear that these complexes can be classified following their value of $|\Delta|$ and the number of pyridines in the coordination sphere of the Fe^{III}. Those exhibiting the larger values of $|\Delta|$ (ca. 14) contain four or five pyridines in the ancillary ligand. Those exhibiting weaker values of $|\Delta|$ (ca. 11) possess three pyridines in the

(35) Griffith, J. S. *The theory of transition metal ions*; Cambridge University Press: London, 1961.

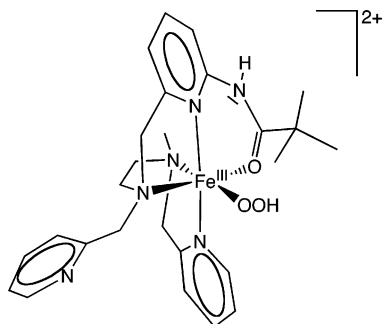
(36) Taylor, C. P. S. *Biochim. Biophys. Acta* **1977**, *491*, 137–149.

(37) Sobolev, A. P.; Babushkin, D. E.; Talsi, E. P. *Mendeleev Commun.* **1996**, 236.

(38) Hazell, A.; McKenzie, C. J.; Nielsen, L. P.; Schindler, S.; Weitzer, M. *J. Chem. Soc. Dalton Trans.* **2002**, 310–317.

Scheme 4. Griffith–Taylor Analysis for Some Low-Spin Non-Heme FeOOH Complexes with Neutral Ligands^a

^a Upper right: representation of the energy diagram in the t_{2g} subset. Lower right: orientation of the g tensor. The values indicated are those of $[(L_5^2aH)Fe^{III}(OOH)]^{2+}$. Left $V = f(-\Delta)$ diagram, V and Δ being in units of the spin-orbit coupling constant λ . Letter code for the ligands:¹⁹ (a) L_5^2aH ; (b) L_5^2 ; (c) TPEN; (d) $L^{3,10}$ (e) $L^{2,10}$ (f) L_5^3 ; (g) Trispicen; (h) TPA; (i) N4Py; (j) $(bpy)_2(py)$; (k) Py5; (l) $(phen)_2(py)$; (m) Bz-tpen.³⁸

Scheme 5. Proposed Structure for $[(L_5^2aH)Fe^{III}(OOH)]^{2+}$ 

ligand. This fact could be interpreted in the following terms:⁷ the larger the number of pyridines bound to the Fe^{III} , the more accepting the metal center and the stronger the interaction with the donor π^* orbital of the hydroperoxo. This interpretation is quite consistent with the variation of the hydroperoxo-to-the Fe^{III} t_{2g} charge-transfer energy as a function of the number of pyridines (see above).

In Scheme 4, the point (a) relative to $[(L_5^2aH)Fe^{III}(OOH)]^{2+}$ is not found in one of the former areas. This argument strengthens the structure proposed above for this complex, i.e., with two amino, the oxygen atom of the pivaloylamidopyridyl fragment and only two pyridines coordinated to the metal center. This structure is shown in Scheme 5.

As shown by the series of UV–vis spectra in Figure 6, the formation of this complex involves another intermediate with a broad absorption at ca. 700 nm. Both intermediates form at the same time when H_2O_2 is added to complex **1**. However, at some point, the 700 nm chromophore is converted to the $Fe^{III}(OOH)$, as revealed by the presence of an isosbestic point at 610 nm. We have observed that the equilibrium between both intermediates was dependent on the pH of the solution. The full identification of the 700 nm chromophore is under investigation in our laboratory.

Conclusion

Two new Fe^{II} complexes have been obtained by using the new ligand L_5^2aH . These complexes exhibit very similar

structures with five nitrogen and one oxygen atom in the coordination sphere of Fe. The first complex is dicationic with the neutral ligand, whereas the second one is monocationic with the deprotonated ligand. In acetonitrile, each complex can be converted into the other following an acid/base equilibrium. The complex with the neutral ligand, formulated as $[(L_5^2aH)Fe^{II}]^{2+}$ reacts with H_2O_2 to give a purple-reddish intermediate. This intermediate has been identified as $[(L_5^2aH)Fe^{III}(OOH)]^{2+}$ where the metal center is low spin and surrounded by four nitrogen and the amide carbonyl oxygen atom of the ligand. Thus, it does not exhibit the conventional “all nitrogen” ancillary ligand that prevails in this family of complexes. This peculiar environment for the Fe center is revealed by the electronic absorption and EPR characteristics of the complex. This complex is in equilibrium with another yet unidentified intermediate, following an acid/base reaction.

Experimental Section

Starting Materials. Starting materials were purchased from Acros. Solvents were purchased from VWR and used without any purification. Preparation and handling of air-sensitive materials (complex synthesis) were carried out under inert atmosphere by using standard Schlenk and vacuum line techniques.

X-ray Crystallography. X-ray diffraction data for **1** were collected by using a Kappa X8 APPEX II Bruker diffractometer with graphite-monochromated Mo $K\alpha$ radiation ($\lambda = 0.71073 \text{ \AA}$). The temperature of the crystal was maintained at the selected value (100 K) by means of a 700 series Cryostream cooling device to within an accuracy of ± 1 K. The data were corrected for Lorentz polarization and absorption effects. The structures were solved by direct methods using SHELXS-97³⁹ and refined against F^2 by full-matrix least-squares techniques using SHELXL-97⁴⁰ with anisotropic displacement parameters for all non-hydrogen atoms. Hydrogen atoms were located on a difference Fourier map and introduced into the calculations as a riding model with isotropic thermal parameters. All calculations were performed by using the Crystal Structure crystallographic software package WINGX.⁴¹

X-ray diffraction data for **2** was recorded on Bruker AXS-Enraf-Nonius Kappa-CCD diffractometer using a graphite monochromator ($\lambda(\text{Mo } K\alpha)$, 0.71073 \AA). The temperature of the crystal was maintained at the selected value 150(1) K using a 700 series Cryostream cooling device. The data were corrected for Lorentz polarization effects. Then, the data were processed using the TeXsan program package.⁴² The structure was solved by direct methods with the use of the SIR92 software⁴³ and refined against F by full-matrix least-squares techniques using TeXsan. The final refinement involved an anisotropic model for all non-hydrogen atoms. The hydrogen atoms were set geometrically. They were recalculated before the last refinement cycle.

The drawing of the two molecules was realized with the help of ORTEP32.⁴⁴ Crystallographic data (excluding structure factors) have

(39) Sheldrick, G. M. *SHELXS-97, release 97-2*; University of Göttingen: Göttingen, Germany, 1998.

(40) Sheldrick, G. M. *SHELXL-97, release 97-2*; University of Göttingen: Göttingen, Germany, 1998.

(41) Farrugia, L. J. *J. Appl. Crystallogr.* **1999**, *32*, 837–838.

(42) *TEXSAN, release 1.7*; Molecular Structure Corporation: The Woodlands, TX, 1992–1997.

(43) Altomare, A.; Cascarano, G.; Giacovazzo, C.; Guagliardi, A. *J. Appl. Crystallogr.* **1993**, *26*, 343–350.

(44) Farrugia, L. J. *J. Appl. Crystallogr.* **1997**, *30*, 565.

been deposited at the Cambridge Crystallographic Data Center as supplementary publications no. CCDC-613014 and -613015. Copies of the data can be obtained free of charge on application to CCDC, 12 Union Road, Cambridge CB21EZ, UK. Fax (+44) 1223-336-033; e-mail: deposit@ccdc.cam.ac.uk.

Electronic Absorption Spectra. Spectra were recorded using a Varian Cary 50 spectrophotometer equipped with a Hellma immersion probe and fiber-optic cable. Low temperature experiments were conducted using a Thermo Haake CT90L cryostat.

Electrospray Ionization Mass Spectrometry (ESI-MS). Spectra were recorded on a Micromass Quattro II or a Thermo Finnigan MAT 95S.

9.4 GHz EPR Spectra. Spectra were recorded on frozen solutions at liquid helium or liquid nitrogen temperatures on a Bruker Elexsys 500 spectrometer. The concentration of the low-spin Fe^{III} complex were determined by double integration of the spectra recorded at 5 K by using the software Xepr. A 1 mM $\text{CuSO}_4 \cdot 5\text{H}_2\text{O}$ stock solution in 2 M HCl, and 2 M $\text{NaClO}_4 \cdot 5\text{H}_2\text{O}$ was used to prepare standards with 1, 0.75, 0.5, and 0.25 mM Cu^{II} , respectively.

Elemental Analyses. Analyses were carried out at the Services de Microanalyse, ICSN-CNRS, Gif-sur-Yvette, France.

Electrochemical Measurements were performed with an EGG PAR (model 273A) electrochemical workstation. The solvents were distilled under argon in the presence of CaH_2 and the solution (2 mM for complexes and 0.2 M of tetrabutylammonium perchlorate (TBAClO_4)) introduced within an argon-purged heart-shaped cell. Cyclic voltammetry was performed using a glassy carbon electrode (3 mm in diameter) as the working electrode and an Ag/AgClO_4 (electrode in acetonitrile) as the reference ($E_{\text{ref}} = 0.3 \text{ V/SCE}$). The low temperature experiments were conducted using a Julabo FP 50 cryostat.

Resonance Raman. Spectra were recorded using a Dilor XY spectrograph, equipped with a liquid-nitrogen-cooled CCD camera. The excitation wavelength was 568 nm (Kr+ Laser) with 5 mW power at the sample. Resonance Raman experiments were carried out at low temperature ($-80 \text{ }^\circ\text{C}$) using a cryostat.

Synthesis of 2-Pivaloylamido-6-methylpyridine (i). To a mixture of 21.6 g (0.2 mol) of 2-amino-6-methylpyridine and 1.3 equiv of triethylamine in 200 mL of CH_2Cl_2 was added dropwise 1.1 equiv of pivaloyl chloride with constant stirring for 2 h at room temperature. Some water was then added to the resulting mixture, and after extraction with CH_2Cl_2 , organic fractions were dried over Na_2SO_4 and filtered. The solvent was then removed by rotary evaporation to afford a whitish solid (94%). $\text{C}_{11}\text{H}_{16}\text{N}_2\text{O}$: 191.3 g mol^{-1} . $^1\text{H NMR}$ (200 MHz, CDCl_3 , δ from TMS): 1.3 (s, 9H), 2.4 (s, 3H), 6.9 (d, 1H), 7.6 (t, 1H), 7.9 (s, 1H), 8 (d, 1H).

Synthesis of 2-Pivaloylamido-6-bromomethylpyridine (ii). **i** (4.6 g, 0.024 mol) was dissolved in 300 mL of degassed CCl_4 , 1 equiv of *N*-bromosuccinimide (4.3 g, 0.024 mol), and AIBN were added under Ar. The mixture was heated to reflux with constant stirring for 6 h under light irradiation. The orange mixture was cooled at room temperature and filtered through a bed of celite to eliminate degradation salts. The solvent was removed by rotary evaporation, and the oil was purified by column chromatography on silica gel (ethyl acetate). The resulting dark brown oil was used for the next step (33%). $\text{C}_{11}\text{H}_{15}\text{BrN}_2\text{O}$: 271.2 g mol^{-1} . $^1\text{H NMR}$ (250 MHz, CDCl_3 , δ from TMS): 1.3 (s, 9H), 4.4 (s, 2H), 6.9–8.2 (m, 3H), 8.3 (s, 1H).

Synthesis of *N*-Methyl-*N,N'*-2-pyridylmethyl-1,2-diamine (v). Bispicen **iii** was prepared by refluxing for 10 min 2 equiv of 2-pyridinecarboxaldehyde (23 mL, 0.24 mol) and 1 equiv of 1,2-ethylenediamine (8 mL, 0.12 mol) in 60 mL of methanol. After

cooling, 24 g of (0.64 mol) of NaBH_4 was slowly added in an ice bath under stirring. The mixture was then heated to reflux with constant stirring for 1 night. After extraction with CH_2Cl_2 , organic fractions were dried over Na_2SO_4 and filtered. The solvent was removed by rotary evaporation to afford a pure yellow oil of **iii** (85%). $\text{C}_{14}\text{H}_{18}\text{N}_4$: 242.3 g mol^{-1} . $^1\text{H NMR}$ (250 MHz, CDCl_3 , δ from TMS): 2.3 (s, 2H), 2.6 (s, 4H), 3.8 (s, 4H), 7.0 (t, 2H), 7.2 (d, 2H), 7.6 (d, 2H), 8.4 (d, 2H).

HCHO (6.4 mL, 25 equiv) (38% in water) was added to a solution of 2.2 g (0.009 mol) of **iii** in 50 mL of methanol with constant stirring for 1 night at room temperature. After extraction with CH_2Cl_2 , organic fractions were dried over Na_2SO_4 and filtered. The solvent was removed by rotary evaporation to afford a pure brown oil of **iv** (97%). $\text{C}_{15}\text{H}_{18}\text{N}_4$: 254.3 g mol^{-1} ; $^1\text{H NMR}$ (250 MHz, CDCl_3 , δ from TMS): 2.9 (s, 4H), 3.4 (s, 2H), 3.8 (s, 4H), 7–8.5 (m, 8H).

A small excess of NaBH_3CN (0.012 mol) was slowly added to a solution of 2.9 g (0.011 mol) of **iv** dissolved in 50 mL of methanol, with constant stirring. CF_3COOH (2 equiv, 2 mL, 0.022 mol) was then added, and the mixture was stirred at room temperature for 5 h. After addition of 100 mL of 4 N NaOH, the mixture was extracted with CH_2Cl_2 to afford a pure brown oil of **v** (54%). $\text{C}_{15}\text{H}_{20}\text{N}_4$: 256.4 g mol^{-1} ; $^1\text{H NMR}$ (250 MHz, CDCl_3 , δ from TMS): 2.2 (s, 3H), 2.6 (t, 2H), 2.7 (t, 2H), 3.6 (s, 2H), 3.8 (s, 2H), 7–8.5 (m, 8H).

Synthesis of 2,2-Dimethyl-*N*-[6-([2-(methyl-pyridin-2-yl-methyl-amino)-ethyl]-pyridin-2-ylmethyl-amino)-methyl]-pyridin-2-yl-propionamide (vi). To a mixture of 1.4 g of **v** (0.005 mol) and 1 equiv of **ii** in CH_3CN were added 6 g of dry K_2CO_3 . The mixture was heated to $80 \text{ }^\circ\text{C}$ for 3 h and then cooled at room temperature. K_2CO_3 was filtered off, the solvent was removed under reduced pressure, and the resulting dark brown oil was purified by column chromatography on silica gel (first with diethyl ether, and then with methanol, the pure compound was collected as the last fraction) to afford a pure brown oil (25%). $\text{C}_{26}\text{H}_{34}\text{N}_6\text{O}$: 446.6 g mol^{-1} . $^1\text{H NMR}$ (250 MHz, CDCl_3 , δ from TMS): 1.2 (s, 9H), 2.1 (s, 3H), 2.7 (m, 4H), 3.6 (s, 2H), 3.7 (s, 2H), 3.8 (s, 2H), 7–8.5 (m, 11H), 8 (s, 1H).

Synthesis of $[(\text{L}_5^2\text{aH})\text{Fe}^{\text{II}}](\text{BPh}_4)_2$ (1-(BPh}_4)_2**).** A solution of 128 mg (0.38 mmol) of $\text{Fe}^{\text{II}}(\text{BF}_4)_2 \cdot 6\text{H}_2\text{O}$ in 6 mL of methanol was added under inert atmosphere to a solution of 177 mg (0.38 mmol) of L_5^2aH in a minimum of methanol. A yellow solid was precipitated upon addition of a concentrated solution of 285.2 mg (2.2 equiv; 0.83 mmol) of NaBPh_4 in methanol under Ar. The precipitate was collected by filtration under inert atmosphere to afford a yellow solid. Yield: 60%. ESI-MS: $m/z = 251$ (M^{2+}). $\text{C}_{74}\text{H}_{74}\text{B}_2\text{FeN}_6\text{O} \cdot 2\text{H}_2\text{O}$ (1140.9 g mol^{-1}): calcd C 75.5, H 6.7, N 7.1; found C 74.2, H 6.3, N 7.5.

Synthesis of $[(\text{L}_5^2\text{aH})\text{Fe}^{\text{II}}](\text{PF}_6)_2$ (1-(PF}_6)_2**).** A solution of 79.5 mg (0.2 mmol) of $\text{Fe}^{\text{II}}(\text{BF}_4)_2 \cdot 6\text{H}_2\text{O}$ in 4 mL of methanol was added under inert atmosphere to a solution of 93.3 mg (0.2 mmol) of L_5^2aH in a minimum of methanol. The solution was orange colored. A concentrated solution of NaPF_6 in $\approx 800 \mu\text{L}$ of methanol was then added. The solution was then concentrated, and a solid was precipitated upon addition of 4 mL of diethyl ether. A greenish solid was collected by filtration under inert atmosphere. Yield: 68%. ESI-MS: $m/z = 251$ (M^{2+}), 501 (M^+). $\text{C}_{26}\text{H}_{34}\text{F}_{12}\text{FeN}_6\text{OP}_2$ (792.4 g mol^{-1}): calcd (M + 2NaPF₆) C 27.7, H 3.1, N 7.4; found C 27.7, H 3.1, N 7.5.

The same complex can be obtained by the following method. L_5^2aH (72.5 mg, 0.16 mmol) was deprotonated using the Huenig's base in methanol. The solution was then degassed and a solution of 1 equiv of $\text{Fe}^{\text{II}}(\text{BF}_4)_2 \cdot 6\text{H}_2\text{O}$ (54.8 mg) in 4 mL of methanol was

Fe(II) Complexes with a New Aminopyridyl Ligand

added under inert atmosphere. A saturated solution of KPF_6 in methanol was added, and the solution was concentrated. Degassed diethyl ether (15 mL) was added, and the mixture was cooled at $-17\text{ }^\circ\text{C}$ but only a little amount of solid was obtained after filtration. A saturated solution of NH_4PF_6 and diethyl ether were still added on the filtrate. After concentration of the solution and filtration of the yellow precipitate, yellow crystals were obtained by cooling the filtrate at $-17\text{ }^\circ\text{C}$ for 2 days.

Synthesis of $[(\text{L}_5\text{-}^2\text{a})\text{Fe}^{\text{II}}]\text{BPh}_4$ (2-(BPh₄)). Deprotonation of the amide function was achieved by treating 248.2 mg of $\text{mL}_5\text{-}^2\text{aH}$ (0.55 mmol) with triethylamine at room temperature. A solution of 185.8 mg (0.55 mmol) of $\text{Fe}^{\text{II}}(\text{BF}_4)_2 \cdot 6\text{H}_2\text{O}$ in 5 mL of methanol was then added under stirring. Precipitation occurred upon addition of 1.2

equiv (227.9 mg, 0.67 mmol) of NaBPh_4 in 3 mL of methanol. A red solid was collected by filtration under Ar. Yield: 51%. After dissolving the precipitate in acetonitrile, dark red crystals of $[(\text{L}_5\text{-}^2\text{a})\text{Fe}^{\text{II}}]\text{BPh}_4$ were obtained by slow evaporation under Ar. ESI-MS: $m/z = 501$ (M^+). $\text{C}_{50}\text{H}_{53}\text{BFeN}_6\text{O} \cdot 2\text{H}_2\text{O}$ (820.6 g mol^{-1}): calcd C 70.1, H 6.7, N 9.8; found C 70.3, H 6.3, N 9.7.

Supporting Information Available: Table S1 contains EPR g values for $S = 1/2$ FeOOH complexes and parameters of the Griffith–Taylor model. This material is available free of charge via the Internet at <http://pubs.acs.org>.

IC0623415